resonant window dimension together with the resonant frequency calculated from (1). It can be noted that the results from the two approaches coincides well with each other with a difference of about one to two percent. Since a discrepancy of a few percent are expected between the result from (1) and that of experiment [6], the results obtained by the present numerical method can be considered to be of good accuracy. Equation (1) is an empirical one which considers only the effect of the dominant mode and it is not likely to give good results when the operating frequency approaches the cutoff frequency of the next higher order mode. This phenomenon can also be observed in Fig. 3. For the curve $a_1/a = 0.7$ when λ/a approaches unity (the cutoff wavelength of the TE_{20} mode) the difference between the two curves becomes bigger. Here again, only two or three basis functions are included in the computation.

In the course of the numerical calculation the most time consuming procedure is the matrix inversion. The size of the matrix to be inverted is determined by the number of the used basis function. Two or three basis functions imply that the matrix to be inverted is of the order 2×2 or 3×3. The numerical analysis with the suggested basis functions is consequently very computationally time saving. The typical CPU time required for one point calculation with as much as 1600 total waveguide modes is about 20 seconds on a CONVEX computer.

IV. Conclusion

A new class of simple-form basis functions are presented for solving waveguide iris coupling problem by using the moment method. A study for different coupling structures using these basis functions shows good agreement with the already published results. Compared with the basis functions published before the basis functions introduced here are characterised by their simple forms, generality and fast convergence which are consequently suitable for analysing relatively complex coupling structures.

References

[1] N. Marcuvitz, *Waveguide Handbook* New York: McGraw-Hill, 1951.
[2] V. P. Lyapin, V. S. Mikhalevsky and G. P. Sinyavsky, "Taking into account the edge condition in the problem of diffration waves on step discontinuity in plate waveguide," *IEEE Trans Microwave Theory Tech*, vol. MTT-20, pp. 763–764, 1972.
[3] M. S. Leong, P. S. Kooi and Chandra, "A new class of basis functions for the solution of the E-plane waveguide discontinuity problem," *IEEE Trans Microwave Theory Tech.*, vol. MTT-35, pp. 705–509, 1987.
[4] H. Auda and R. F. Harrington, "A moment solution for waveguide junction problems," *IEEE Trans Microwave Theory Tech.*, vol. MTT-31, pp. 515–519, 1983.
[5] L. A. Weinstein, "The theory of diffraction and the factorization method," in *Generalzed Wiener-Hopf Technique*, Boulder, CO: Golem, 1969.
[6] Chen, Tsung-Shan, "Characteristics of waveguide resonant iris filters," *IEEE Trans Microwave Theory Tech.*, pp. 260–262, Apr. 1967.

Numerical Electromagnetic Inverse-Scattering Solutions for Two-Dimensional Infinite Dielectric Cylinders Buried in a Lossy Half-Space

S. Caorsi, G. L. Gragnani, and M. Pastorino

***Abstract*—An approach to microwave imaging in a half-space geometry and for infinite dielectric cylinders buried in a lossy medium is proposed. The two-dimensional integral-equation for the inverse-scattering problem is discretized by the moment method. The resulting ill-conditioned system is solved by pseudoinversion. A multi-incidence process based on the invariance of the Green matrix to the incident field is described. Results of some numerical simulations, assuming a noisy environments, are reported and discussed.**

I. Introduction

In this paper, a two-dimensional integral formulation of inverse scattering in a half-space is proposed for microwave imaging of buried objects. This technique is of great interest in many geophysical and civil-engineering fields. Detection of cables and pipes (plastic materials) is a significant example. In the past, some works dealt with the problem of identifying nonmetallic structures by radar [1], [2], and an interesting method for microwave imaging of buried objects was proposed in [3]. Moreover, a diffraction tomography methodology previously developed for medical applications, was proposed for electromagnetic imaging of buried cylindrical inhomogeneities [4].

In the present paper, the theory of inverse scattering is applied to solve the integral equation, whose unknown terms are the products of the object functions by the total electric field. After considering an equivalent current density to model the investigation domain, the resulting integral equations are solved numerically by the moment method (MoM) [5].

In the last few years, several moment-method-based inverse-scattering solutions for many different situations have been presented. Ghodgaonkar *et al.* [6] developed a method for imaging 3-D biological targets; Ney *et al.* [7] used the pseudoinversion transformation to retrieve the polarization current in mono- and two-dimensional scatterers. Moreover, two works by Guo and Guo [8], [9] furnished a theoretical background to develop reconstruction algorithms. Finally, the authors of the present paper proposed an approach to the reconstruction of unknown dielectric scatterers in free space [10]. In this work, the possibility of determining the dielectric properties of unknown objects buried in a half-space is explored. Input data are obtained by measuring the values of the scattered electric field inside an observation domain located near the boundary between the different media. A TM-wave incident electric field is used to illuminate the unknown objects. A multi-illumination-angle imaging process is proposed. Since the Green matrix is invariant to the incident electric field vector, this multi-illumination process does not require an increase in computational resources. Another interesting feature lies in the possibility of computing off line (and once for all) the pseudoinverse matrix, after fixing the investigation and observation domains.

Manuscript received March 2, 1992; revised May 28, 1992.

The authors are with the Department of Biophysical and Electronic Engineering, University of Genoa, Via all'Opera Pia, 11A, 16145 Genoa, Italy.

IEEE Log Number 9204497.

II. Mathematical Model

Let us consider the cylindrical geometry presented in Fig. 1. S is a fixed investigation area on a plane orthogonal to the cylinder axis (i.e., parallel to the z axis) and buried in region 2. It contains, at an unknown position, the cross section of a cylindrical object whose shape and complex dielectric permittivity are unknown. The dielectric properties of the scatterer may vary with the transverse coordinates only. The media of regions 1 and 2 are characterized by the complex dielectric permittivities $\epsilon_1^* = \epsilon_0[\epsilon_{r1} - j(\omega\epsilon_0)^{-1}\sigma_1]$ and $\epsilon_2^* = \epsilon_0[\epsilon_{r2} - j(\omega\epsilon_0)^{-1}\sigma_2]$. The magnetic permeability is μ_0 everywhere. The unknown complex dielectric permittivity inside the area S can be expressed as $\epsilon_S^*(x,y) = \epsilon_0[\epsilon_{rS}(x,y) - j(\omega\epsilon_0)^{-1}\sigma_S(x,y)]$ for $(x,y) \in S$. Let us assume a set of TM-wave incident electric field vectors in region 1, i.e., $\boldsymbol{E}_{\text{inc}}^i(x,y) = \Psi_{\text{inc}}^i(x,y)\boldsymbol{z}, i = 1,\cdots,I$. Due to reflection and transmission by and through the boundary plane, the following Helmholtz equations hold for that region:

$$[\nabla_t^2 + k_1^{*2}][\Psi_{\text{inc}}^i(x,y) + \Psi_{\text{ref}}^i(x,y) + \Psi_{\text{scatt}}^{1i}(x,y)] = 0 \qquad y > 0, i = 1,\cdots,I \tag{1}$$

where: $\boldsymbol{E}_{\text{ref}}^i(x,y) = \Psi_{\text{ref}}^i(x,y)\boldsymbol{z}$ (electric field vectors reflected by the boundary plane), $\boldsymbol{E}_{\text{scatt}}^{1i}(x,y) = \Psi_{\text{scatt}}^{1i}(x,y)z$ (electric field vectors scattered by the inhomogeneities in region S), and $k_1^{*2} = \omega\mu_0\epsilon_1^*$. Inside the lower medium, equivalent current densities, $\boldsymbol{J}_{\text{eq}}^i(x,y) = K_{\text{eq}}^i(x,y)\boldsymbol{z}, i = 1,\cdots,I$, are used to model region S. So, for region 2, the following Helmholtz equations hold:

$$[\nabla_t^2 + k_2^{*2}][\Psi_{\text{trans}}^i(x,y) + \Psi_{\text{scatt}}^{2i}(x,y)] = j\omega\mu_0 K_{\text{eq}}^i(x,y) \qquad y < 0, i = 1,\cdots,I \tag{2}$$

where: $\boldsymbol{E}_{\text{trans}}^i(x,y) = \Psi_{\text{trans}}^i(x,y)\boldsymbol{z}$ (electric field vectors transmitted through the boundary plane), $\boldsymbol{E}_{\text{scatt}}^{2i}(x,y) = \Psi_{\text{scatt}}^{2i}(x,y)\boldsymbol{z}$ (electric field vectors scattered by the inhomogeneities in region S), and $k_2^{*2} = \omega\mu_0\epsilon_2^*$. The equivalent current densities are related to the dielectric properties of region S via the following relation:

$$\begin{aligned} K_{\text{eq}}^i(x,y) &= j(\omega\mu_0)^{-1}[k_S^{*2}(x,y) - k_2^{*2}] \cdot [\Psi_{\text{trans}}^i(x,y) + \Psi_{\text{scatt}}^{2i}(x,y)] \\ &= o(x,y)[\Psi_{\text{trans}}^i(x,y) + \Psi_{\text{scatt}}^{2i}(x,y)] (x,y) \in S \end{aligned} \tag{3}$$

In this relation, the term $k_S^{*2}(x,y) = \omega\mu_0\epsilon_S^*(x,y)$ and $o(x,y)$, independent of the index i, is called the *object function* (or *scattering potential*). The measured scattered electric fields can be espressed in integral form [11]:

$$\iint_S K_{\text{eq}}^i(x',y')\,\Gamma_h^{21}(x,y,x',y')\,dx'\,dy' = \Psi_{\text{scatt}}^{1i}(x,y) \qquad y > 0, i = 1,\cdots,I \tag{4}$$

where the Green function for the half-space geometry [11] can be written as

$$\Gamma_h^{21}(x,y,x',y') = \frac{1}{2\pi}\int_{-\infty}^{-\infty} \frac{j}{\gamma_1+\gamma_2}\exp\{-j\lambda[x-x']\} \cdot \exp\{\gamma_1 y - \gamma_2 y'\}\,d\lambda \tag{5}$$

where $\gamma_1 = (\lambda^2 - k_1^{*2})^{1/2}$ and $\gamma_2 = (\lambda^2 - k_2^{*2})^{1/2}$, with $\text{Im}\{\gamma_1\} \le 0$ and $\text{Im}\{\gamma_2\} \le 0$. Relation (4) is an integral equation with the unknown $K_{\text{eq}}(x',y')$. Assuming to measure the total electric field (and to derive the scattered electric field) at M testing points in region 1, we can apply the MoM to (4) (assuming piecewise basis functions) [5]:

$$\sum_{n=1}^{N} K_n^i \iint_{S_n} \Gamma_h^{21}(x_m,y_m,x',y')\,dx'\,dy' = \Psi_{\text{scatt}}^{1i}(x_m,y_m) \qquad m = 1,\cdots,N \quad i = 1,\cdots,I \tag{6}$$

where the values K_n^i are the coefficients of the series expansions $\Sigma_{n=1}^N K_n^i u(x,y)$, with $u(x,y) = 1$, if $(x,y) \in S_n$, and $u(x,y) = 0$, otherwise. The kernel of (4) is invariant to the incident field (i.e., it is independent of i), and this property is kept in the systems of equations (6), which can be written in matrix form as

$$[\Gamma^{21}]\underline{K}^i = \underline{\Psi}_{\text{scatt}}^{1i} \qquad i = 1,\cdots,I \tag{7}$$

where the arrays $\underline{K}^i$ and $\underline{\Psi}_{\text{scatt}}^{1i}$ are given by $\underline{K}^i = [K_1^i, K_2^i, \cdots, K_N^i]^T$ and $\underline{\Psi}_{\text{scatt}}^{1i} = [\Psi_{\text{scatt}}^{1i}(x_1,y_1), \Psi_{\text{scatt}}^{1i}(x_2,y_2), \cdots, \Psi_{\text{scatt}}^{1i}(x_M, y_M)]^T, i = 1,\cdots,I$. As a consequence, the matrix elements of $[\Gamma^{21}]$ can be calculated only once, and the arrays $\underline{K}^i, i = 1,\cdots,I$, can be obtained by applying a pseudoinversion algorithm, as it has previously been done for imaging in free space [7], [10] to overcome the ill-conditioning. We obtain:

$$\underline{K}^i = [\Gamma^{21}]^+\underline{\Psi}_{\text{scatt}}^{1i} \qquad i = 1,\cdots,I \tag{8}$$

where $[\Gamma^{21}]^+$ is the pseudoinverse matrix of $[\Gamma^{21}]$. It can be derived off line and once for all (independently of the number of incident electric fields used). By means of the reconstructed equivalent current densities, we can obtain the dielectric properties by using relation (3), where the values of Ψ_{scatt}^{2i} are computed, in an approximate way, in terms of the coefficient K_n^i in (9) at the bottom of this page, where

$$\begin{aligned} \Gamma_h^{22}(x,y,x',y') &= \frac{1}{2\pi}\int_{-\infty}^{-\infty}\frac{j}{2\gamma_2}\frac{\gamma_2-\gamma_1}{\gamma_1+\gamma_2}\exp\{-j\lambda[x-x']\} \cdot \exp\{-j\gamma_2(y+y')\}\,d\lambda + \frac{1}{2\pi}\int_{-\infty}^{-\infty}\frac{j}{2\gamma_2} \\ &\quad \cdot \exp\{-j\lambda[x-x']\}\exp\{-j\gamma_2|y+y'|\}\,d\lambda \end{aligned} \tag{10}$$

where $\gamma_1 = (\lambda^2 - k_1^{*2})^{1/2}$ and $\gamma_2 = (\lambda^2 - k_2^{*2})^{1/2}$, with $\text{Im}\{\gamma_1\} \le 0$ and $\text{Im}\{\gamma_2\} \le 0$. It should be noted that the coefficients $\{\iint_{S_n}\Gamma_h^{22}(x,y,x',y')\,dx'\,dy'\}$ can be evaluated off line and once for all, too, and stored in a computer memory. If we assume constant dielectric parameters inside each subdomain $S_n, n = 1,\cdots,N$, from relations (9) and (3) we obtain (11) at the bottom of the next page, where (x_n,y_n) indicates the center of the subdomain S_n, whose constant dielectric permittivity is ϵ_S^{*n}.

$$o(x,y) = I^{-1}\sum_{i=1}^{1}\frac{\sum_{n=1}^{N}K_n^i u(x,y)}{\Psi_{\text{trans}}^i(x,y) + \sum_{n=1}^{N}K_n^i\iint_{S_n}\Gamma_h^{22}(x,y,x',y')\,dx'\,dy'} \qquad i = 1,\cdots,I \tag{9}$$

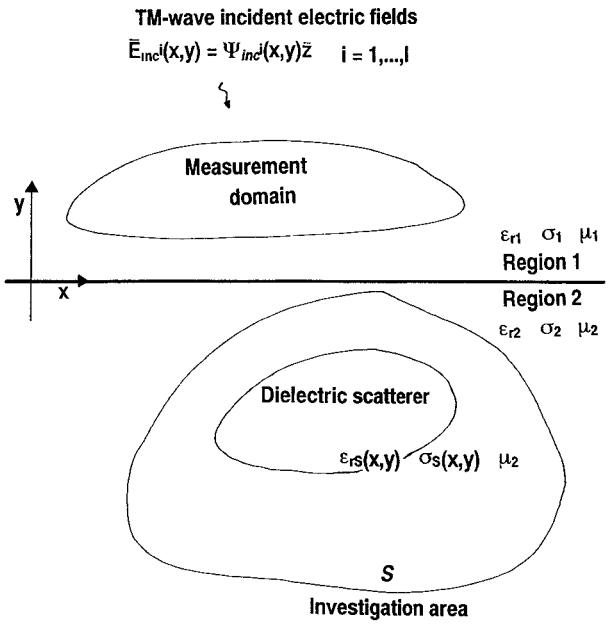

Fig. 1. Problem geometry.

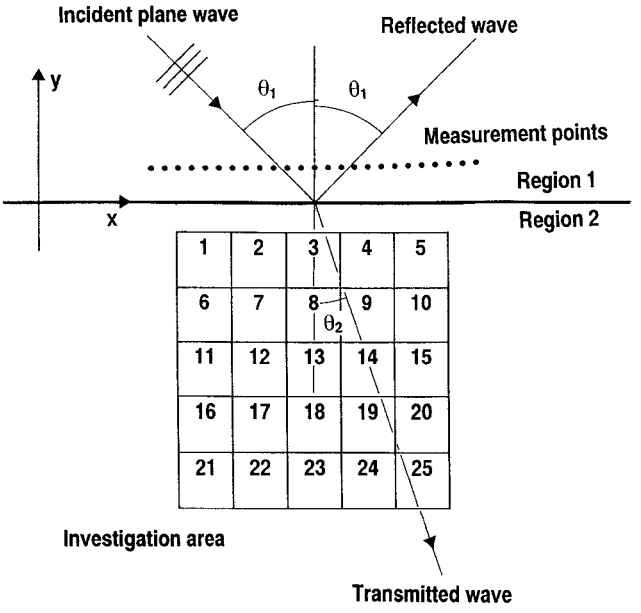

Fig. 2. Geometrical configuration adopted for the numerical simulations.

III. Numerical Simulations and Discussion

Let us consider the geometrical configuration shown in Fig. 2. The investigation area was assumed to be of square shape and to measure $\lambda\sqrt{5}/3 \times \lambda\sqrt{5}/3$, where λ was the wavelength in region 1. The area was partitioned into 25 $\lambda/3\sqrt{5} \times \lambda/3\sqrt{5}$-sided subareas, and the distance between the upper side of this domain and the boundary plane was assumed to be equal to $\lambda/6\sqrt{5}$. Twenty-five equally-spaced ($\lambda/10\sqrt{5}$) measurement points were arranged on a line placed in region 1 at a distance $\lambda/6\sqrt{5}$ (Fig. 2). A square homogeneous scattering object was assumed to occupy a whole subarea. For the first simulations, the dielectric parameters of the object were $\epsilon_r = 10.0$ and $\sigma = 0.0$, and we assumed $\epsilon_{r1} = 1.0$ and $\sigma_1 = 0.0$ for region 1 and $\epsilon_{r2} = 5.0$ and $\sigma_2 = 0.0$ for region 2. A transmitted wave obtained through the normal incidence ($\theta_1 = \theta_2 = 0$) of a uniform unit plane wave upon region 1 illuminated the scatterer. The scattered electric field at each measurement point was calculated by solving the EFIE, following a procedure analogous to the one used by Richmond [12] for TM scattering in free space.

In the first set of simulations, we performed dielectric reconstructions for different positions of the scattering object inside the investigation domain. Fig. 3 gives the histograms of the percentage errors on the reconstructions of the equivalent-current-density amplitudes and of the relative dielectric permittivities at some significant locations inside the subarea containing the scatterer (refer to the cell numbering in Fig. 2). As can be seen, a very good reconstruction was achieved when the scatterer was assumed to occupy cell 1, i.e., to be very close to the boundary plane (about $\lambda/10$). When the scatterer's depth increased, the errors also increased (by about 20–30 percent for a distance from the boundary plane ranging between $\lambda/2\sqrt{5}$ and $3\lambda/2\sqrt{5}$). They increased by about 45 percent for cell 22 (distance equal to $3\lambda/2\sqrt{5}$). As can be seen from Fig. 3, the results of these noiseless simulations show that the reconstruction of the scatterer's dielectric permittivity is almost equivalent for cells 8, 13, 17, while the background appears noisier as the scatterer's depth increases.

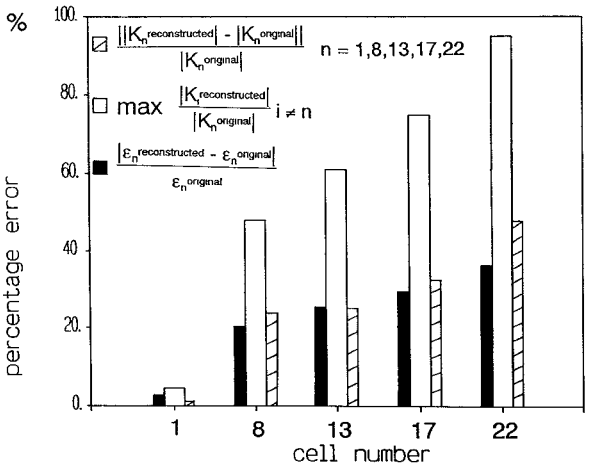

Fig. 3. Percentage errors on the dielectric reconstructions (scatterer: $\epsilon_r = 10.0$ and $\sigma_2 = 0.0$; region 2: $\epsilon_{r2} = 5.0$ and $\sigma_2 = 0.0$; number of incidences: $I = 1, \theta_1 = 0.0$ (rad); S/N = ∞).

In a second set of simulations, we considered an idealized lossy dielectric scatterer ($\epsilon_r = 1.0$ and $\sigma = 10.0$) of the same dimensions as those of the previous lossless scatterer. The results of the reconstruction of the electric conductivity are presented in Fig. 4. The plot

$$\epsilon_S^{*n} = (\omega^2\mu_0)^{-1}\left[k_2^{*2} - j\omega\mu_0 I^{-1}\sum_{i=1}^{I}\frac{\sum_{n=1}^{N} K_n^i u(x,y)}{\Psi_{\text{trans}}^i(x_n,y_n) + \sum_{n=1}^{N} K_n^i \iint_{S_n} \Gamma_h^{22}(x_n,y_n,x',y')\,dx'\,dy'}\right] \qquad i = 1,\cdots,I \tag{11}$$

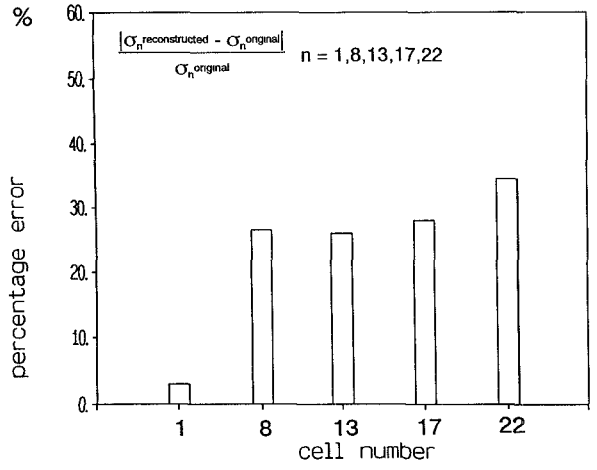

Fig. 4. Percentage errors on the reconstruction of the electric conductivity of the scatterering object (scatterer: $\epsilon_r = 1.0$ and $\sigma = 10.0$; region 2: $\epsilon_{r2} = 5.0$ and $\sigma_2 = 0.0$; number of incidences: $I = 1, \theta_1 = 0.0$ (rad); S/N = ∞).

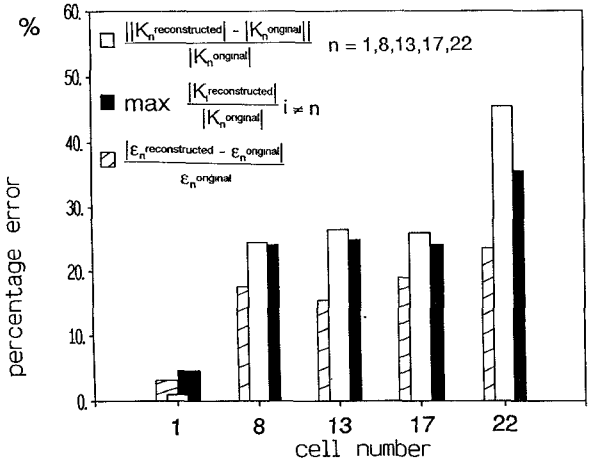

Fig. 5. Percentage errors on the dielectric reconstructions (scatterer: $\epsilon_r = 10.0$ and $\sigma = 0.0$; region 2: $\epsilon_{r2} = 5.0$ and $\sigma_2 = 0.2$; number of incidences: $I = 1, \theta_1 = 0.0$ (rad); S/N = ∞).

shows a certain increase in the reconstruction error as the scatterer's depth increases; for instance, the error increases by about 35 percent for cell 22. By contrast, it is very small for cell 1.

Then, the same scattering object as considered in the first simulations ($\epsilon_r = 10.0$ and $\sigma = 0.0$) was placed in a lossy medium (region 2) characterized by $\epsilon_{r2} = 5.0$ and $\sigma_2 = 0.2$. Fig. 5 gives the results of the dielectric reconstructions. One can notice that both the equivalent current density and the dielectric permittivity of the object were reconstructed quite well (as in the case of the lossless medium), while the background cells were reconstructed far better than shown in Fig. 4. This is to be ascribed to the fact that, in these noiseless simulations, attenuations due to losses in region 2 did not significantly affect the input data from a computational point of view. On the contrary, a different incident-field value (both in amplitude—due to losses—and in phase) for each cell allows us to obtain more informative scattering data at the measurement points. It will be shown that this improvement does not occur in the case of noisy input data.

To evaluate noise effects, a random array made up of two independent sequences of Gaussian noise (zero mean) was added to the same input data, in order to obtain different values of the signal-to-noise

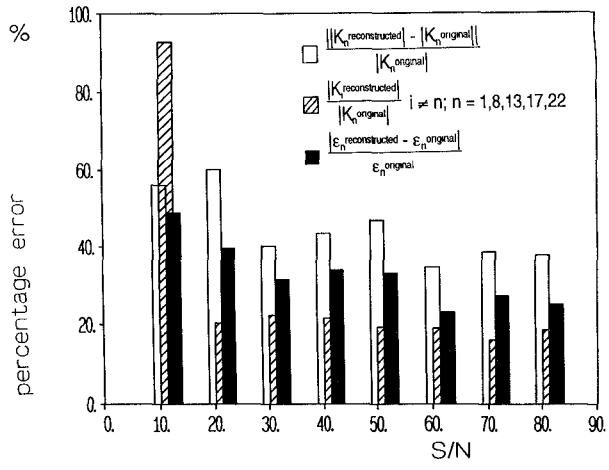

Fig. 6. Percentage errors on the dielectric reconstruction of a scattering object contained in the 8th cell (scatterer: $\epsilon_r = 10.0$ and $\sigma = 0.0$; region 2: $\epsilon_{r2} = 5.0$ and $\sigma_2 = 0.2$; number of incidences: $I = 1, \theta_1 = 0.0$ (rad); S/N = 10, 20, 40, 60, 80 dB.

ratio, S/N. This ratio can be defined as:

$$\mathrm{S/N} = 10 \log \frac{||\underline{\Psi}^{1,}_{\mathrm{scatt}}||2}{||\underline{N}||^2} \tag{12}$$

where $\underline{N}$ indicates the random array. As an example, Fig. 6 shows the reconstruction errors versus different values of the signal-to-noise ratio (10–80 dB) for cell 8. We assumed the same scatterer ($\epsilon_r = 10.0$ and $\sigma = 0.0$) and the same lossy medium ($\epsilon_{r2} = 5.0$ and $\sigma_2 = 0.2$). The data on the equivalent current density are affected by percentage errors greater than 40 percent, for S/N < 60 dB. Nevertheless, the reconstruction of the dielectric permittivity can be considered acceptable (percentage errors smaller than 50 percent). Instead, notable errors affect the data on the background cells for the lowest values of the S/N ratio.

A certain improvement was obtained through a multi-incidence process. Since the Green matrix is independent of the incident electric field, one can use more than one illumination, and then average the obtained values, without significantly increasing the computational load (as the pseudoinverse matrix is computed off line and once for all). We considered 5 incident uniform plane waves, propagating with angles $\theta_1 = 0, 0.25, 0.5, 0.75, 1$ (rad). The scatterer ($\epsilon_r = 10.0$ and $\sigma = 0.0$) was located in the 17th cell, and the propagation medium was characterized by $\epsilon_{r2} = 5.0$ and $\sigma_2 = 0.2$. Fig. 7 gives the values of the reconstructed dielectric permittivity of the scattering object in the whole investigation domain (for S/N = 20 dB): the plot (a) refers to the single-incidence process, and the plot (b) refers to the 5-incidence process. Only a slight improvement in the reconstruction of the dielectric permittivity of the scatterer was obtained in this case (about 6.6 for 5 incidences vs. 6.2 for 1 incidence). However, in general, no advantages of the multi-incidence process can be noticed in the results of the scatterer reconstruction. Nevertheless, this technique allows one to obtain more regular background reconstructions. These results are better pointed out in Table I, which gives the mean errors on the reconstructions of the dielectric permittivities inside the empty cells, together with the largest error, which is related to the worst-reconstructed cell, for S/N ranging between 20 and 80 dB. It should be noted that a further improvement might result from considering at least the symmetrical incidence angles ($\theta_1 = -0.25, -0.5, -0.75, -1.0$ (rad)). Finally, Table II gives, for completeness, the partial results of each single-incidence solution, obtained for each illumination angle ($\theta_1 = 0.0, 0.25, 0.5, 0.75, 1.0$ (rad)) and for the same values of the S/N

TABLE I
VALUES OF THE RECONSTRUCTED RELATIVE DIELECTRIC PERMITTIVITY FOR $I = 1, \theta_1 = 0\ 0$ (rad) AND $I = 5, \theta_1 = 0, 0, 0.25, 0.5, 0.75, 1.0$ (rad). SCATTERER: $\epsilon_r = 10.0$ AND $\sigma = 0.0$; REGION 2: $\epsilon_{r2} = 5.0$ AND $\sigma_2 = 0\ 2$; S/N = 20, 40, 60, 80 dB

Signal-to-noise ratio	Number of incidences	$\max_k \lvert\epsilon_r^{rec}(k) - \epsilon_r^{orig}(k)\rvert$	$N^{-1}\sum_k^1 \lvert\epsilon_r^{rec}(k) - \epsilon_r^{orig}(k)\rvert$
S/N = 80 dB	P = 1	0.7	0.2
	P = 5	0.5	0.12
S/N = 60 dB	P = 1	1.2	0.21
	P = 5	0.4	0.11
S/N = 40 dB	P = 1	1.2	0.25
	P = 5	0.7	0.13
S/N = 20 dB	P = 1	0.5	0.16
	P = 5	0.6	0.11

TABLE II
VALUES OF THE RECONSTRUCTED RELATIVE DIELECTRIC PERMITTIVITY FOR $I = 1, \theta_1 = 0.0, \theta_1 = 0.25, \theta_1 = 0.5, \theta_1 = 0.75, \theta_1 = 1\ 0$ (PARTIAL RESULTS OF EACH SINGLE -INCIDENCE PROCESS). SCATTERER: $\epsilon_r = 10.0$ AND $\sigma = 0.0$; REGION 2: $\epsilon_{r2} = 5.0$ AND $\sigma_2 = 0.2$; S/N = 20, 40, 60, 80 dB

	S/N = 80 dB	S/N = 60 dB	S/N = 40 dB	S/N = 20 dB
θ = 0 0 rad	0.266	0 293	0 140	0 381
θ = 0 25 rad	0.278	0 287	0 350	0 376
θ = 0 5 rad	0.291	0 291	0 271	0 275
θ = 0 75 rad	0.295	0 295	0 314	0 298
θ = 1 0 rad	0 298	0 302	0 309	0.410

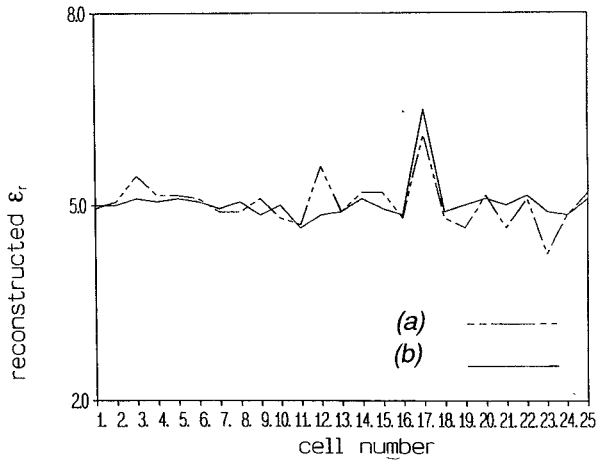

Fig. 7. Reconstructed relative dielectric permittivity in the investigation domain. Number of incidences: (continuous line) $I = 1, \theta_1 = 0.0$ (rad); (dashed line) $I = 5, \theta_1 = 0, 0, 0.25, 0.5, 0.75, 1.0$ (rad). (scatterer: $\epsilon_r = 10\ 0$ and $\sigma = 0.0$; region 2: $\epsilon_{r2} = 5.0$ and $\sigma_2 = 0.2$; S/N = 20 dB).

ratio. As expected, the reconstruction quality is entirely independent of the illumination angle, due to the infinite wavefront of the incident plane wave used as an interrogating wave.

IV. CONCLUSIONS

An approach to microwave imaging of two-dimensional infinite dielectric cylinders buried in a half-space configuration has been proposed. The approach is based on an integral formulation of e.m. scattering in terms of the Green function for two half-space (seminfinite) homogeneous dielectric media interfaced by a plane. The MoM and a pseudoinversion algorithm are used in the numerical scheme. A multi-incidence process makes it possible to obtain a reduction in the reconstructed background noise, with no increase in the required computational resources, thanks to the invariance of the Green matrix to the incidence angle.

Numerical results show that dielectric reconstructions are feasible, even though errors are to be expected, especially for lower values of the signal-to-noise ratio and for deeper objects.

REFERENCES

[1] K. Iizuka and A. P. Freundofer, "Detection of nonmetallic buried objects by a step-frequency radar," *Proc. IEEE*, vol. 67, pp. 991–1000, July 1979.
[2] L. C. Chen *et al.*, "Improved performance of a subsurface radar target identification system through antenna design," *IEEE Trans. Antennas Propagat.*, vol. AP-29, pp. 307–311, Mar. 1981.
[3] N. Osumi and K. Ueno, "Microwave holographic imaging of underground objects," *IEEE Trans. Antennas Propagat.*, vol. AP-33, pp. 152–159, Feb. 1985.
[4] L. Chommeloux, C. Pichot, and J. Bolomey, "Electromagnetic modeling for microwave imaging of cylindrical buried inhomogeneities," *IEEE Trans. Microwave Theory Tech*, vol. MTT-34, no. 10, Oct. 1986.
[5] R. F. Harrington, *Field Computation by Moment Method.* New York: Macmillan, 1968.
[6] D. K. Ghodgaonkar, O. P. Gandhi, and M. J. Hagmann, "Estimation of complex permittivities of three-dimensional inhomogeneous biological bodies," *IEEE Trans. Microwave Theory Tech.*, vol. MTT-31, pp. 442–446, 1983.
[7] M. M. Ney, A. M. Smith, and S. S. Stuchly, "A solution of electromagnetic imaging using pseudoinverse transformation," *IEEE Trans. Med. Imaging*, vol. MI-3, pp. 155–162, 1984.
[8] T. C. Guo and W. W. Guo, "Computation of electromagnetic wave scattering from an arbitrary three-dimensional inhomogeneous dielectric object," *IEEE Trans Magn*, vol. 38, pp. 99–106, 1990.
[9] ——, "Three-dimensional dielectric imaging by inverse scattering with resolution unlimited by wavelength," in *Ann Rep. Conf Electrical Insulation and Dielectric Phenomena*. Leesburg, VA, 1989, pp. 65–74.
[10] S. Caorsi, G. L. Gragnani, and M. Pastorino, "Two-dimensional microwave imaging by numerical inverse scattering solution," *IEEE Trans Microwave Theory Tech*, vol. 38, pp. 981–989, 1990.
[11] A. Sommerfeld, *Partial Differential Equation* New York: Academic Press, 1949.
[12] J. H. Richmond, "Scattering by a dielectric cylinder of arbitrary cross-section shape," *IEEE Trans Antennas Propagat.*, vol. AP-13, pp. 334–341, 1965.

Calculating Input Impedance of Electrically Small Insulated Antennas for Microwave Hyperthermia

Piotr S. Debicki and Melvin A. Astrahan

Abstract— **Two analytical methods for approximating the input impedance of insulated monopole or dipole antennas embedded within an electrically dense medium have been reported in the literature. The methods differ by the applied degree of approximation in the solution of the integral equation for the current in the insulated conductor. These methods directly affect the calculation of the wavenumber and the characteristic impedance of an antenna treated as a lossy coaxial line. In the more complex approach the resulting formulas contain an additional term which improves the correlation with measured and numerically modeled results for electrically longer antennas. When applied to electrically small antennas (i.e. $< 1/8$ wavelength in the medium), this term introduces a significant error into the calculation of the real part of the complex input impedance. Special care must be taken if these formulas are used to design multisectional antennas in order to avoid impedance mismatch. Two methods for correcting this error are presented.**

I. Introduction

Insulated dipole and monopole antennas embedded in a dissipative dielectric medium may be found in many technical areas including communications, physical measurements, geophysical exploration and localized heating. An important medical application of localized heating is hyperthermic therapy of cancer and certain benign diseases [2]–[5], [9] where insulated antennas are often used as interstitial and intracavitary hyperthermia applicators.

Two analytical approximations which describe the current distribution and input impedance of these antennas have been developed by King *et al.* [6]–[8]. We will refer to these approximations as the *insulated antenna theory* (IAT). According to the IAT, the insulated antenna embedded in a lossy dielectrtic is treated as a lossy transmission line terminated with an ideal open end which assumes infinite terminating impedance. The transmission parameters of the line are derived from approximate solutions of the integral equation for the current along the antenna.

The methods differ bya the applied degree of approximation in the solution of the integral equation for the current in the insulated conductor and also differ slightly in assumptions. These results directly affect calculation of the wavenumber of the current and the characteristic impedance of an antenna treated as a lossy coaxial line. The simpler approximation [7], although appropriate for electrically smaller antennas ($h < 1/4$ wavelength in the surrounding medium—λ_M) leads to significant error as h becomes longer. The more complex (MC) approach [7] contains an additional term which improves the correlation with measured and numerically modeled results for electrically longer antennas. When applied to electrically small antennas (i.e. $< 1/8\lambda_M$), this additional term introduces a significant error into the calculation of the real part of the complex input impedance.

Iskander and Tumeh [3] have proposed an iterative approach to designing multisectional antennas based on the MC method of approximating the current distribution. If their approach is used to develop devices (such as hyperthermia applicators) containing multisectional antennas special care must be taken to avoid impedance matching error.

Manuscript received May 24, 1991; revised June 17, 1992.

The authors are with the Norris Cancer Hospital, Radiation Oncology Dept., University of Southern California, Los Angeles CA 90033.

IEEE Log Number 9204498.

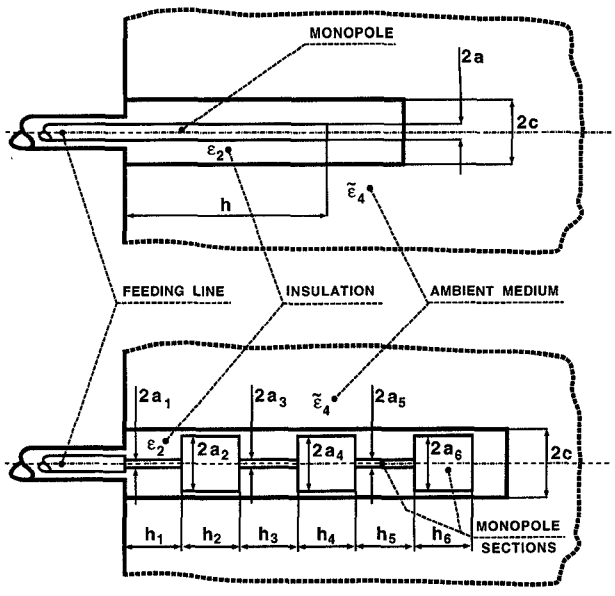

Fig. 1. Insulated antenna embedded in an electrically dense medium. Uniform monopole (at top). Sectorial antenna in the form used in Table I (at bottom).

II. Methods

The IAT was used to compare the two approximation methods for electrically small antennas. Consider the case of a monopole antenna with lossless insulation and time dependence $e^{j\omega t}$. The insulated monopole (Fig. 1(a) consists of a perfect central conductor of length h and outer diameter (OD) $2a$. This is surrounded by an insulating layer with OD = $2c$. The monopole is assumed to be ideally open ended. The insulation may consist of one or two layers. However, for simplicity, only a single layer will be considered. Outside the insulation there is an infinite ambient medium. The wavenumber of the insulating layer is $k_2 = \omega(\mu_0\epsilon_2)^{1/2}$ and the wavenumber of the ambient medium is $k_4 = \beta_4 - j\alpha_4 = \omega(\mu_0\tilde{\epsilon}_4)^{1/2}$.

The assumptions of the IAT are that the cross section of the antenna is electrically small ($(k_2c)^2 \ll 1$) and that the electric density ($|k_i|$) of the ambient medium is higher than that of the insulation. In the MC case $|k_4/k_2|^2 \geq 2$ and in the less complex (LC) approximation $|k_4/k_2|^2 \geq 16$.

The input impedance of the monopole antenna can be calculated from the complex wavenumber (k_L) and the complex characteristic impedance Z_c of the line:

$$Z_{\text{in}} = -jZ_c/\tan(k_Lh) \tag{1}$$

In the case of LC approximation of the current distribution:

$$k_L = k_2[1 + F/\ln(c/a)]^{1/2} \tag{2}$$

$$Z_c = k_L\ln(c/a)/(2\pi\omega\epsilon_2) \tag{3}$$

where $F = H_0^{(2)}(k_4c)/[k_4cH_1^{(2)}(k_4c)]$. The MC approach yields:

$$k_L = k_2[1 + F/\ln(c/a)]^{1/2}[1 + (F(k_2/k_4)^2/\ln(c/a))]^{-1/2} \tag{4}$$

$$Z_c = k_L\ln(c/a)/(2\pi\omega\epsilon_2) + k_LF(k_2/k_4)^2/(2\pi\omega\epsilon_2) \tag{5}$$